



THE UNIVERSITY *of* EDINBURGH

Edinburgh Research Explorer

Second group of high-pressure high-temperature lanthanide polyhydride superconductors

Citation for published version:

Sun, W, Kuang, X, Keen, HDJ, Lu, C & Hermann, A 2020, 'Second group of high-pressure high-temperature lanthanide polyhydride superconductors', *Physical review B*, vol. 102, 144524.
<https://doi.org/10.1103/PhysRevB.102.144524>

Digital Object Identifier (DOI):

[10.1103/PhysRevB.102.144524](https://doi.org/10.1103/PhysRevB.102.144524)

Link:

[Link to publication record in Edinburgh Research Explorer](#)

Document Version:

Peer reviewed version

Published In:

Physical review B

General rights

Copyright for the publications made accessible via the Edinburgh Research Explorer is retained by the author(s) and / or other copyright owners and it is a condition of accessing these publications that users recognise and abide by the legal requirements associated with these rights.

Take down policy

The University of Edinburgh has made every reasonable effort to ensure that Edinburgh Research Explorer content complies with UK legislation. If you believe that the public display of this file breaches copyright please contact openaccess@ed.ac.uk providing details, and we will remove access to the work immediately and investigate your claim.



Second group of high-temperature lanthanide polyhydride superconductors under high pressure

Weiguo Sun,^{1,2,3} Xiaoyu Kuang,² Harry D. J. Keen,³ Cheng Lu,^{1,*} and Andreas Hermann^{3,†}

¹*School of Mathematics and Physics, China University of Geosciences (Wuhan), Wuhan 430074, China*

²*Institute of Atomic and Molecular Physics, Sichuan University, Chengdu 610065, China*

³*Centre for Science at Extreme Conditions and SUPA, School of Physics and Astronomy, University of Edinburgh, Edinburgh, EH9 3FD, United Kingdom*

(Dated: October 7, 2020)

Rare-earth polyhydrides formed under pressure are promising conventional superconductors, with the critical temperature T_c in compressed LaH₁₀ almost reaching room temperature. Here, we report a systematic computational investigation of the structural and superconducting properties of rare-earth (RE) polyhydrides formed under pressure across the whole lanthanide series. Analyses of the electronic and dynamical properties and electron-phonon coupling interaction for the most hydrogen-rich hydrides REH_{*n*} ($n = 8, 9, 10$) that can be stabilized below 400 GPa show that enhanced T_c correlates with a high density of H *s*-states and low number of RE *f*-states at the Fermi level. In addition to previously predicted and measured LaH₁₀ and CeH₉, we suggest YbH₁₀ and LuH₈ as additional potential high- T_c superconductors. They form a ‘second island’ of high- T_c superconductivity amongst the late lanthanide polyhydrides, with an estimated T_c of 102 K for YbH₁₀ at 250 GPa.

Metallic hydrogen has been suggested as a potential conventional high-temperature superconductor [1]. Although hydrogen is predicted to become metallic and have high superconducting critical temperature T_c at pressures beyond 450 GPa [2, 3], it is still a challenge to achieve such immense pressure in experiments, and the most recent studies report somewhat diverging properties of compressed hydrogen [3–5]. Meanwhile, Ashcroft suggested that ‘chemical precompression’ of hydrogen in hydride materials would lead to metallization at much lower pressures [6]. As a consequence, theoretical calculations have predicted a wide range of promising pressure induced metallic hydrides [7–14], such as sodalite-like clathrate CaH₆ and YH₆, where predicted T_c values reach about 235 and 290 K at 150 and 300 GPa, respectively [7, 14]. Hydrogen sulfide was first theoretically reported as a good candidate for high- T_c superconductivity [15–17], before experiments confirmed that H₃S has a T_c of 203 K at pressures of 155 GPa [18]. The excellent agreement between theory and experiment greatly increased confidence in computational predictions. Encouraging results have spurred a flurry of interest in other compressed hydrides, that is, solid materials containing hydrogen atoms bonded to other elements for related hydrides with both higher T_c and potentially broader ranges of stability [19–22].

Peng *et al.* have reported stable hydrogen-rich (H-rich) compounds with clathrate structures by using crystal structure prediction on rare-earth (RE) metallic hydrides under extreme conditions [23]. They found that clathrate H-rich hydrides allow high H content with purely atomic character, i.e. no H₂ molecules, and highlighted the cubic phase LaH₁₀ with a H₃₂ cage and surprisingly high T_c of 288 K at 200 GPa. The calculated T_c for sodalite-like fcc YH₁₀ is predicted to reach about 326 K, above

room-temperature [20–23], elevating the class of H-rich hydrides to potential room-temperature superconductors [24, 25]. Most recently, experiments by Drozdov *et al.* [26] and Somayazulu *et al.* [27] have established LaH₁₀ as the highest measured T_c , reaching 250 K at 170 GPa, setting the current record of superconducting T_c near room-temperature. While stability of the various RE polyhydrides had been studied by Peng *et al.* [23] across the entire lanthanide series of elements, superconductivity properties have only been reported for the early RE hydrides of La, Ce, and Pr. Calculations of electronic and T_c properties have accompanied recent experimental reports on syntheses of individual RE polyhydrides, CeH₉ [28, 29], PrH₉ [30, 31], NdH₉ [32], EuH₉ [33] and ThH₁₀ [24]. However, a systematic investigation of electron-phonon coupling and superconducting T_c across all RE hydrides is missing. A theoretical analysis of hydride superconductivity across the periodic table by Semenok *et al.* [34] used a neural network model to predict low T_c across the lanthanide series, as increasing numbers of RE *f*-electrons at the Fermi level can weaken the electron-phonon coupling (EPC) interaction and suppress superconductivity.

In this article, we present a systematic study of potential hydride superconductivity across the entire lanthanide series, focusing on the most H-rich RE hydride species stabilized by each RE element under pressure. We mainly focus on the H-rich clathrate REH_{*n*} ($n = 8, 9, 10$) hydride structures with atomic H₂₄, H₂₈, H₂₉, and H₃₂ cages and perform systematic studies of their energetic, dynamical, and electronic properties. Electronic structure properties reveal that large density of H-like electronic states at the Fermi level (N_{ef}) correlates with high superconducting T_c , while increasing the relative contribution of RE *f*-electrons is associated with

weakening of EPC interaction. This leads to a strong suppression of T_c in the middle of the lanthanide series but also a ‘second island’ of superconductivity in the late lanthanides, as we show that the late RE hydrides YbH_{10} and LuH_8 (which become stable between 250 and 300 GPa) also have potential for high-temperature superconductivity ($T_c \sim 100$ K). We propose that H-rich hydrides of late lanthanides, with fully filled f -shells, should not be overlooked by experimental groups who attempt to synthesize the various RE polyhydrides.

We conducted crystal structure searches for the early lanthanide hydrides using the particle swarm optimization method as implemented in the CALYPSO package [35–37], focusing on the REH_n ($n = 3-10$) stoichiometries at 100, 150, 200, 250, 300 and 400 GPa. Subsequently, all candidate structures from our own searches combined with previous reports [23, 34] were applied across the whole lanthanide series and the full 100-400 GPa pressure range. The validity of CALYPSO in structure prediction has been demonstrated for various systems which have been confirmed by experiment [15, 20, 23, 38], including high pressure lanthanide hydrides [20, 23]. The underlying total energy calculations and structure optimizations were performed at density functional theory (DFT) level of theory as implemented in the Vienna Ab Initio Simulation Package (VASP) [39]. Projector augmented wave (PAW) potentials with $5s^2 5p^6 6s^2 (5d, 4f)^n$ valence spaces were used to represent the electron-ion interactions [39, 40]. The Perdew-Burke-Ernzerhof (PBE) [41] functional was employed for exchange-correlation effects. Plane wave bases with cutoff energy of 800 eV and dense k -point meshes with $2\pi \times 0.03 \text{ \AA}^{-1}$ spacing gave excellent convergence of the structural relaxations and electronic calculations.

The electronic band structures, electron density of states (DOS) and electron-phonon coupling were determined using density functional perturbation theory (DFPT) as implemented in the QUANTUM-ESPRESSO code [42]. Ultrasoft pseudopotentials for lanthanide rare-earth RE and H atoms were chosen and plane wave cutoff energy was 80 Ry. For calculations of superconducting electron-phonon coupling (EPC) parameter λ , the Brillouin zone was sampled using a $4 \times 4 \times 4$ ($4 \times 4 \times 2$) q -point mesh and much denser $24 \times 24 \times 24$ ($32 \times 32 \times 16$) k -point mesh for cubic (hexagonal) hydrides structures. The superconducting critical temperature (T_c) was estimated by solving the Allen-Dynes modified McMillan equation [43], which has been shown to give very good results in compressed metal hydrides [16, 23]. In our calculation, Coulomb pseudopotential $\mu^* = 0.1$ and 0.13 were used.

We explored the energetically stable phases of lanthanide hydrides (REH) at high pressures by constructing the relevant convex hulls. In Figs. 1, S1 and S2 in the Supplementary Information (SI), the convex hulls and resulting pressure-composition phase diagrams for

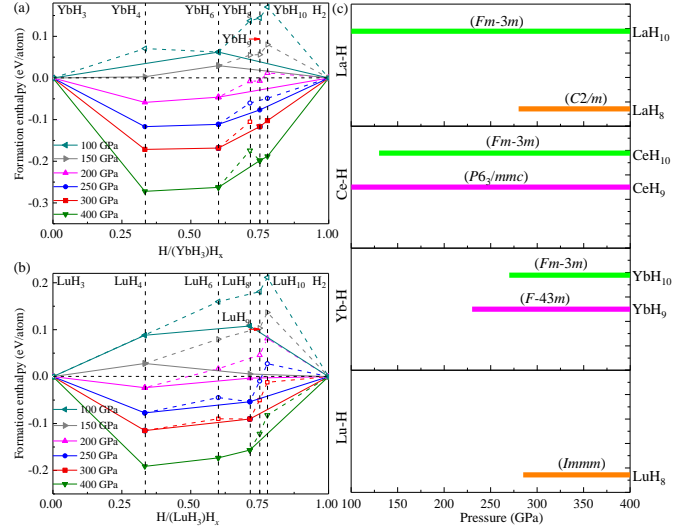


FIG. 1: (a, b) Convex hull construction for polyhydrides Yb-H and Lu-H phases relative to REH_3 and H_2 under pressure range from 100 to 400 GPa, filled (open) symbols represent the stable (metastable) phases. (c) Stability pressure-composition H-rich phase diagram of REH_n (RE = La, Ce, Yb, Lu; $n = 8, 9, 10$) systems.

all RE hydrides are shown relative to REH_3 and H_2 and across the pressure range from 100 to 400 GPa. For all lanthanides, REH_4 is a stable structure. For almost all lanthanides, REH_{10} is stable at high pressures (exceptions are Ho, Er, Tm, and Lu), and usually REH_9 , in a cubic or hexagonal structure, becomes stable at slightly lower pressures (the exception is La, where LaH_{10} is very stable at relatively low pressures already). The sodalite-like REH_6 ($Im\bar{3}m$) phase emerges as an additional stable structure from Pm onwards. The first stable REH_8 stoichiometry is predicted for NdH_8 , which also occurs as preferred stable clathrate structure (> 250 GPa) in the late lanthanide hydrides of Ho, Er, Tm and Lu. With the exception of orthorhombic ($Immm$) LuH_8 , all other REH_8 hydrides are stable in a cubic $Fm\bar{3}m$ phase. The most hydrogen-rich RE hydrides are therefore (at least up to 400 GPa) either REH_8 , REH_9 , or REH_{10} . For early RE hydrides La and Ce, we have reproduced the various structures (including LaH_{10} and CeH_9), which have been experimentally synthesised under high pressure [26–29]. The predicted mid-lanthanide structures are in agreement with the results by Peng *et al.* [23]: the most H-rich clathrate hydride REH_{10} is stabilised across RE = Nd, Pm, Sm, Eu, Gd, Tb, and Dy. For the late lanthanide systems of Er, Tm, Yb and Lu hydrides, the ErH_8 , TmH_8 , YbH_{10} and LuH_8 phases emerged as stable hydrides at pressures above 250 GPa, which complements prior theoretical and experimental work [20, 23, 28]. As illustration, the thermodynamic convex hull construction for polyhydrides YbH_n and LuH_n at different pressures is depicted in Fig. 1(a, b), from which the clathrate hy-

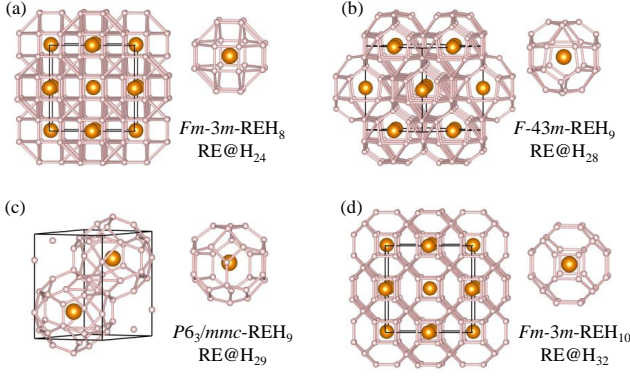


FIG. 2: Crystal structures of lanthanide polyhydrides and corresponding RE-centered H cages. Small (large) spheres represent H (RE) atoms. (a) $Fm\bar{3}m$ REH₈, (b) $F\bar{4}3m$ REH₉, (c) $P6_3/mmc$ REH₉ and (d) $Fm\bar{3}m$ REH₁₀.

hydrides $Fm\bar{3}m$ YbH₁₀, $F\bar{4}3m$ YbH₉ and $Immm$ LuH₈ are predicted as stable structures under high pressure. The corresponding pressure-composition diagrams of REH_{*n*} (RE = La, Ce, Yb, Lu, *n* = 8, 9, 10) are shown in Fig. 1(c).

In Fig. 2, we have shown the four relevant, stable H-rich clathrate structures, which include $Fm\bar{3}m$ REH₈, $F\bar{4}3m$ REH₉, $P6_3/mmc$ REH₉ and $Fm\bar{3}m$ REH₁₀. In $Fm\bar{3}m$ REH₈ hydrides (Fig. 2(a)), H₂₄ cages surround the central metal atoms; this is the most H-rich phase found in the Nd, Ho, Er, and Tm hydride systems. The $Immm$ LuH₈ structure is a small distortion of this structure type. In the cubic phase ($F\bar{4}3m$) for REH₉ in Fig. 2(b), H₂₈ cages surround the central atoms; this structure appears at some conditions as the most H-rich hydride in the Pr, Nd, Pm, Sm, Ho and Yb systems. Meanwhile, H₂₉ cage structures in hexagonal phase REH₉ Fig. 2(c) appear stable in Ce, Eu, Gd, Tb and Dy hydrides. Lastly, in the cubic $Fm\bar{3}m$ REH₁₀ structure formed by most RE elements (see above), H₃₂ cages surround every metal atom (Fig. 2(d)). The absence of imaginary phonons in the dispersion curves (Fig. S3 and S4) confirms the dynamical stability of all predicted polyhydrides.

From here on, we focus on the properties of the predicted most H-rich REH_{*n*} (*n* = 8, 9, 10) clathrate hydrides structures for each RE element. The electronic density of states (DOS) calculations of these phases (Figs. 3 and S5) confirm their metallic character across the series. As shown in Fig. S5, the striking narrow $4f$ -band of electronic states moves from above the Fermi level (LaH₁₀, CeH₉) to below the Fermi level (YbH₁₀, LuH₈) along the lanthanide series. The inset figures in Fig. S5 show the electronic DOS around the Fermi level, which are dominated by RE- f and H- s states. Fermi surfaces of all RE hydrides have been displayed in Figs. S6 and S7. The number of projected H- s and RE- f states at the Fermi level for the various H-rich RE hydrides is shown in Fig. 3(a). The projected f -DOS behaves as expected:

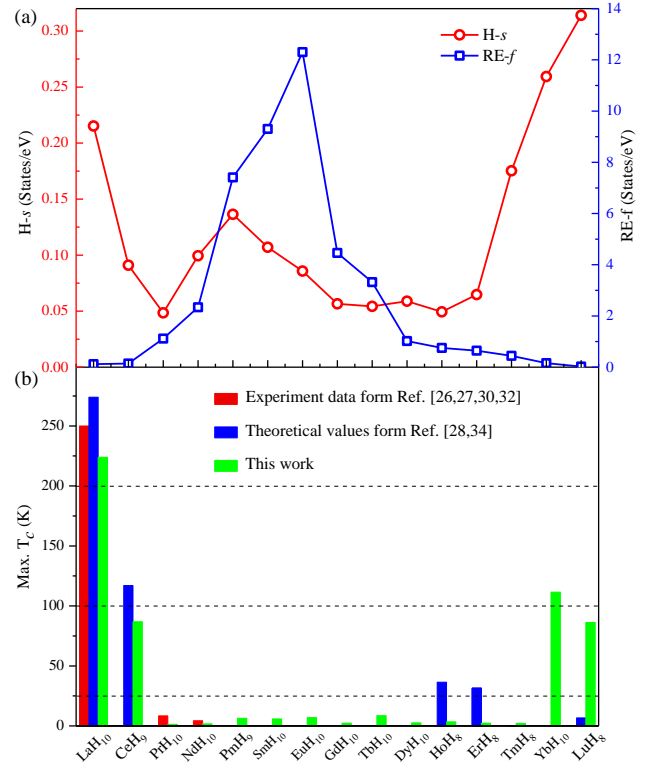


FIG. 3: (a) Calculated electronic DOS of H s -states and RE atom f -states at the Fermi level in different polyhydrides. (b) Maximum T_c for lanthanide polyhydrides, including the experimentally confirmed LaH₁₀ (250 K) [26, 27], PrH₉ (~9 K) [30] and NdH₉ (~4.5 K) [32], and theoretically predicted CeH₉ (117 K) [28], HoH₄ (36.4 K), ErH₁₅ (31.5 K) and LuH₁₂ (6.7 K) [34].

essentially zero for the early RE elements (La, Ce and Pr), the RE f -states increase rapidly with atomic number. A maximum is reached for the Eu-H hydride system (EuH₁₀ structure), which corresponds to a half f -filled [Xe] $6s^2 4f^7$ valence configuration. From Eu-H towards the latter lanthanide hydrides, the RE f -DOS reduces as the $4f$ -states are mainly below the Fermi energy (shown in Fig. S5). For Yb and Lu hydrides, the f -DOS at the Fermi energy is basically zero again. For the H- s states (note different scale in Fig. 3(a)), their presence at the Fermi level decreases with atomic number across the early RE elements, from La to Pr. There is some structure amongst the mid-RE hydrides from Nd-H to Sm-H, but in general the H- s states reach a low plateau only to resurge again for the late RE hydrides of Tm, Yb and Lu. The general trend of electronic DOS of H- s and RE- f states at the Fermi level in the different polyhydrides is (different structures notwithstanding) in agreement with the valence states of RE atoms in lanthanide compounds [44, 45].

The electronic structure in the late RE hydrides (Tm, Yb, Lu) thus mirrors the situation for the early RE hydrides (La, Ce, Pr): a high number of H- s states at

TABLE I: Predicted electron-phonon coupling and superconducting properties of lanthanide polyhydrides at specified pressures, T_c are estimated by McMillan equation.

Element	Polyhydrides	Pressure (GPa)	λ	ω_{log} , K	T_c (K)	
					$\mu^* = 0.10$	$\mu^* = 0.13$
Lanthanum	LaH ₁₀	250	2.25	1444.7	223.9	210.4
Cerium	CeH ₉	250	0.97	1307.1	86.8	74.1
	CeH ₁₀	250	0.59	1983.6	43.8	30.6
Praseodymium	PrH ₁₀	400	0.32	1653.9	1.4	0.3
Neodymium	NdH ₁₀	400	0.35	953.6	1.7	0.5
Cerium	PmH ₉	250	0.34	1326.8	0.9	0.1
	PmH ₁₀	250	0.39	1829.0	6.3	2.5
Samarium	SmH ₉	250	0.36	967.9	2.0	0.6
	SmH ₁₀	250	0.43	993.2	5.8	2.8
Europium	EuH ₆	200	0.33	817.8	0.9	0.2
	EuH ₉	250	0.33	1149.2	1.3	0.3
	EuH ₁₀	250	0.47	723.5	6.9	4.8
Gadolinium	GdH ₁₀	300	0.46	279.4	2.3	1.3
Terbium	TbH ₉	250	0.39	1270.1	4.4	1.8
	TbH ₁₀	400	0.63	325.6	8.5	6.2
Dysprosium	DyH ₉	250	0.27	1399.7	0.2	0.1
	DyH ₁₀	400	0.39	678.2	2.5	1.0
Holmium	HoH ₈	200	0.29	1033.4	0.4	0.1
	HoH ₉	250	0.38	1090.2	3.3	1.3
Erbium	ErH ₈	250	0.35	1335.8	2.3	0.7
Ytterbium	YbH ₉	250	1.02	1112.9	79.6	68.5
	YbH ₁₀	250	1.10	1279.5	102.1	89.2
Lutetium	LuH ₈	300	2.18	565.7	86.2	80.9

the Fermi level and low RE- f character, which could be promising for strong electron-phonon coupling (EPC) and potential superconductivity [1, 46]. We therefore performed the EPC calculations for all H-rich lanthanide polyhydride systems, and collected superconducting properties including the EPC parameters λ , ω_{log} and T_c at different pressures in Table S1 in the SI. In Fig. 3(b), we show our calculated T_c results across the entire lanthanide hydride series. Results for LaH₁₀ and CeH₉ hydrides ($T_c \sim 224$ and 87 K, $\mu^* = 0.1$) are in agreement with the established experimental results [26, 27] and calculations for LaH₁₀ ($T_c \sim 250$ K, $\mu^* = 0.1$) and CeH₉ ($T_c \sim 117$ K, $\mu^* = 0.1$) [28]. The trend for T_c for lanthanide polyhydrides away from La and Ce is strongly downwards. When arriving at RE elements around the half-filled $4f$ states (Eu, Gd, Dy and Ho), the DOS of H- s states reaches the lowest values, while the Re- f states have high values, resulting in weak EPC and low T_c . However, as the atomic number of the lanthanide increases further, a ‘second island’ of superconductivity appears in Yb and Lu polyhydrides, reaching 102 K at 250 GPa in YbH₁₀ (80 K in YbH₉) and 86 K at 300 GPa in LuH₈. The EPC parameters λ for YbH₉ and YbH₁₀ (250 GPa) and LuH₈ (300 GPa) are 1.02, 1.10, and 2.18, re-

spectively, which is larger than those predicted for CeH₉ [28], see Table 1. Our calculations focused on calculations of structurally similar H-rich clathrate hydrides across the entire lanthanide series, REH _{n} ($n = 8, 9, 10$), and indicate the ‘secondary wave’ of superconductivity begins with Yb. There are hints that other structures hold promise as well: Semenuk *et al.* [34] reported an upturn in T_c in latter lanthanide atoms from Ho and Er onwards, with maximum T_c for $I4/mmm$ HoH₄ and $P\bar{6}2m$ ErH₁₅ as 36.7 and 31.5 K ($\mu^* = 0.1$), respectively (see also Fig. 3(b)).

At low pressure, the divalent character of Yb coupled with propensity to valence fluctuations distinguish it from the other lanthanide elements [44, 47–49]. YbH₂ has been reported to undergo a structural and insulator-metal transition by neutron diffraction under high pressure, and suggested that superconductivity emerges at higher pressures with strong EPC driven by enhanced charge fluctuations [48]. As YbH₁₀ leads the ‘secondary wave’ of high-temperature superconductivity in our calculations, we show detailed electronic properties of YbH₁₀ at the single-particle level at 250 GPa in Fig. 4. The electronic band structure and DOS of YbH₁₀ shown in Fig. 4 (a) indicate the metallic character of YbH₁₀

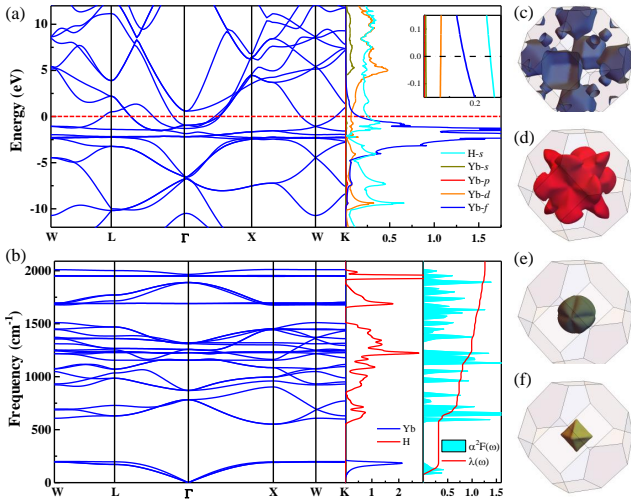


FIG. 4: (a) Calculated electronic band structures and density of states (DOS) of YbH₁₀ at 250 GPa, (b) Phonon dispersion curves, phonon density of states (PHDOS) projected on Yb and H atoms and Eliashberg spectral function $\alpha^2F(\omega)$ together with the electron-phonon integral $\lambda(\omega)$, (c-f) The Fermi surface sheets of YbH₁₀.

with several bands crossing the Fermi level. According to the projected DOS, the main contributions at the Fermi energy come from Yb-*d*, Yb-*f* and H-*s* orbitals (shown as inset in Fig. 4(a)). There is a sharp peak of Yb-*f* states just below the Fermi level. Detailed Fermi surfaces are displayed in Fig. 4(c-f) and agree qualitatively with the Fermi surface of LaH₁₀ (see Fig. S6): three electron pockets around Γ (two very small, one large and with multiple protrusions), and one sizeable hole pocket around X. The appearance of ‘flat band-steep band’ Fermi level crossings [46] and relatively large number of H-*s* states at the Fermi level again indicate YbH₁₀ could display high temperature superconductivity, which is consistent our EPC calculations above ($T_c \sim 102$ K). Phonon dispersion curves for YbH₁₀ structure are displayed in Fig. 4(b), together with projected phonon DOS, the Eliashberg EPC spectral function $\alpha^2F(\omega)$ and the cumulative EPC integral $\lambda(\omega)$. There are two separate phonon frequency ranges: the acoustic phonon modes dominated by Yb atoms below 250 cm⁻¹, which contribute relatively little to the total EPC λ , and H-dominated optical modes above 675 cm⁻¹, vibrations in the clathrate H₃₂ cages, that contribute most to λ . For LuH₈ hydride, the detailed electronic properties and EPC parameters are displayed in a similar way in Fig. 5. The ‘flat band-steep band’ Fermi level crossings also emerge in Fig. 5(c), indicating that LuH₈ could support high temperature superconductivity. Detailed electron-phonon calculation results are shown in Fig. 5(b,d), which result in T_c about 86.2 K, with large EPC $\lambda \sim 2.18$ (see also Table 1). In LuH₈, as broadly found in other high T_c hydrides [19, 20, 28, 50], the high-frequency H-dominated vibrations make the largest con-

tribution to EPC λ and thus sizeable T_c .

Comparing the superconductivity trends across the whole lanthanide hydride series, our results show that, while LaH₁₀ remains the record holder for highest T_c also in our calculations, YbH₁₀ and LuH₈ hydrides should also be considered as potential high temperature superconductors. The H-rich clathrate hydrides with atomic hydrogen cage structures are stable across the entire series at high pressure, and the high-frequency hydrogen sublattice vibrations contribute effectively to strong EPC and enhanced superconductivity. Recently, continuing synthesis efforts have made inroads into the lanthanide series of hydrides, including Pr [30, 31], Nd [32], Eu [33] and Dy [51]. Pushing towards the late lanthanides might add further insight into the limits of BCS superconductivity and the ultimate goal to achieve room-temperature T_c .

In summary, we have systematically explored superconductivity in H-rich REH_{*n*} hydrides for the entire lanthanide hydride series, with combined structure searches and first-principles DFT calculations. We uncovered several new RE-H polyhydride structures with characteristic hydrogen clathrate cages; the most H-rich phases feature H₂₄, H₂₈, H₂₉ and H₃₂ cages in high-symmetry structures REH_{*n*} ($n = 8, 9, 10$), with RE atoms located at the centers of the hydrogen cages. Detailed DOS and EPC calculations for the respective most H-rich phases across the series show that high number of H-*s* states and low number of RE-*f* states at the Fermi level lead to strong EPC interactions and high- T_c superconductivity. To the known LaH₁₀ and CeH₉ hydrides we add YbH₁₀ and LuH₈ at the other end of the series with sizeable predicted T_c . We suggest experimental groups who attempt to synthesize RE polyhydrides with high- T_c explore the ‘second island’ of superconductivity in the late RE polyhydrides.

We acknowledge funding from National Natural Science Foundation of China (No. 11574220, 11874043, 11304167, and U1804121). Computational resources provided by the UK’s National Supercomputer Service through the UK Car-Parrinello consortium (EP-SRC Grant No. EP/P022561/1) and by the UK Materials and Molecular Modelling Hub (No. EP/P020194) are gratefully acknowledged. WS also acknowledges China Scholarship Council (CSC) funding, and HDJK acknowledges PhD studentship support from EPSRC (No. EP/L015110/1).

* Electronic address: lucheng@calypso.cn

† Electronic address: a.hermann@ed.ac.uk

[1] N. W. Ashcroft, Phys. Rev. Lett. **21**, 1748 (1968).

[2] P. Cudazzo, G. Profeta, A. Sanna, A. Floris, A. Continenza, S. Massidda, and E. K. U. Gross, Phys. Rev. Lett. **100**, 257001 (2008).

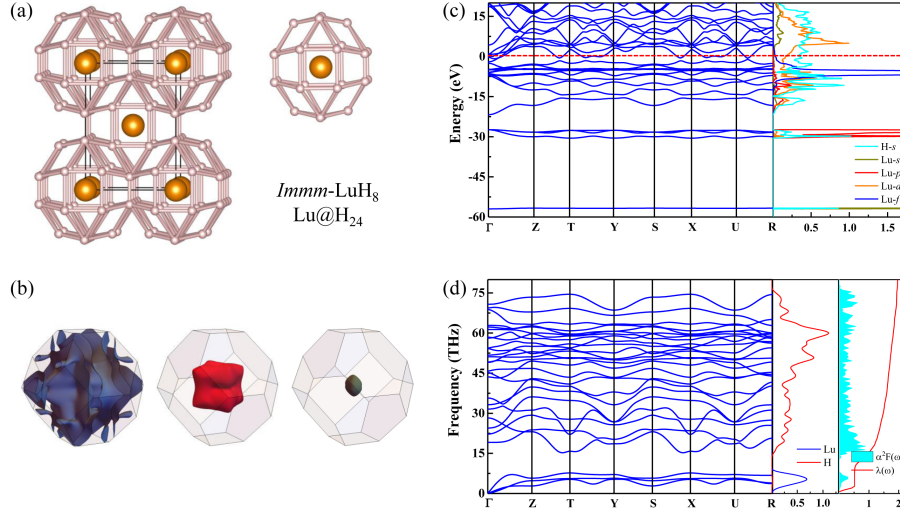


FIG. 5: (a) Crystal structure of *Immm*-LuH₈ at 300 GPa, (b) Fermi surface sheets of LuH₈, (c) Calculated electronic band structures and density of states (DOS) of LuH₈, (d) Phonon dispersion curves, phonon density of states (PHDOS) projected on Lu and H atoms and Eliashberg spectral function $\alpha^2F(\omega)$ together with the electron-phonon integral $\lambda(\omega)$.

- [3] P. Loubeyre, F. Occelli, and P. Dumas, *Nature* **577**, 631 (2020).
- [4] R. P. Dias and I. F. Silvera, *Science* **355**, 715 (2017).
- [5] M. I. Eremets, A. P. Drozdov, P. Kong, and H. Wang, *Nat. Phys.* **15**, 1246 (2019).
- [6] N. W. Ashcroft, *Phys. Rev. Lett.* **92**, 187002 (2004).
- [7] H. Wang, J. S. Tse, K. Tanaka, T. Iitaka, and Y. Ma, *Proc. Natl. Acad. Sci. U. S. A.* **109**, 6463 (2012).
- [8] X. F. Zhou, A. R. Oganov, X. Dong, L. Zhang, Y. Tian, and H. T. Wang, *Phys. Rev. B* **84**, 054543 (2011).
- [9] D. Y. Kim, R. H. Scheicher, C. J. Pickard, R. J. Needs, and R. Ahuja, *Phys. Rev. Lett.* **107**, 117002 (2011).
- [10] P. Baettig and E. Zurek, *Phys. Rev. Lett.* **106**, 237002 (2011).
- [11] D. Y. Kim, R. H. Scheicher, H. K. Mao, T. W. Kang, and R. Ahuja, *Proc. Natl. Acad. Sci. U. S. A.* **107**, 2793 (2010).
- [12] G. Gao, A. R. Oganov, A. Bergara, M. Martinez-Canales, T. Cui, T. Iitaka, Y. Ma, and G. Zou, *Phys. Rev. Lett.* **101**, 107002 (2008).
- [13] M. I. Eremets, I. A. Trojan, S. A. Medvedev, J. S. Tse, and Y. Yao, *Science* **319**, 1506 (2008).
- [14] Y. Li, J. Hao, H. Liu, J. S. Tse, Y. Wang, and Y. Ma, *Sci. Rep.* **5**, 9948 (2015).
- [15] Y. Li, J. Hao, H. Liu, Y. Li, and Y. Ma, *J. Chem. Phys.* **140**, 174712 (2014).
- [16] D. Duan, Y. Liu, F. Tian, D. Li, X. Huang, Z. Zhao, H. Yu, B. Liu, W. Tian, and T. Cui, *Sci. Rep.* **4**, 6968 (2014).
- [17] I. Errea, M. Calandra, C. J. Pickard, J. Nelson, R. J. Needs, Y. Li, H. Liu, Y. Zhang, Y. Ma, and F. Mauri, *Phys. Rev. Lett.* **114**, 157004 (2015).
- [18] A. P. Drozdov, M. I. Eremets, I. A. Troyan, V. Ksenofontov, and S. I. Shylin, *Nature* **525**, 73 (2015).
- [19] X. Zhong, H. Wang, J. R. Zhang, H. Y. Liu, S. T. Zhang, H. F. Song, G. C. Yang, L. J. Zhang, and Y. M. Ma, *Phys. Rev. Lett.* **116**, 057002 (2016).
- [20] H. Liu, I. I. Naumov, R. Hoffmann, N. W. Ashcroft, and R. J. Hemley, *Proc. Natl. Acad. Sci. U. S. A.* **114**, 6990 (2017).
- [21] Y. Quan, S. S. Ghosh, and W. E. Pickett, *Phys. Rev. B* **100**, 184505 (2019).
- [22] X. Zhang, W. Xu, Y. Wang, S. Q. Jiang, F. A. Gorelli, E. Greenberg, V. B. Prakapenka, and A. F. Goncharov, *Phys. Rev. B* **97**, 064107 (2018).
- [23] F. Peng, Y. Sun, C. J. Pickard, R. J. Needs, Q. Wu, and Y. Ma, *Phys. Rev. Lett.* **119**, 107001 (2017).
- [24] A. G. Kvashnin, D. V. Semenok, I. A. Kruglov, I. A. Wrona, and A. R. Oganov, *ACS Appl. Mater. Interfaces* **10**, 43809 (2018).
- [25] D. V. Semenok, A. G. Kvashnin, I. A. Kruglov, and A. R. Oganov, *J. Phys. Chem. Lett.* **9**, 1920 (2018).
- [26] A. P. Drozdov, P. P. Kong, V. S. Minkov, S. P. Besedin, M. A. Kuzovnikov, S. Mozaffari, L. Balicas, F. F. Balakirev, D. E. Graf, and V. B. Prakapenka *et al.*, *Nature* **569**, 528 (2019).
- [27] M. Somayazulu, M. Ahart, A. K. Mishra, Z. M. Geballe, M. Baldini, Y. Meng, V. V. Struzhkin, and R. J. Hemley, *Phys. Rev. Lett.* **122**, 027001 (2019).
- [28] N. P. Salke, M. M. Davari Esfahani, Y. Zhang, I. A. Kruglov, J. Zhou, Y. Wang, E. Greenberg, V. B. Prakapenka, and J. Liu, *et al.*, *Nat. Commun.* **10**, 4453 (2019).
- [29] X. Li, X. Huang, D. Duan, C. J. Pickard, D. Zhou, H. Xie, Q. Zhuang, Y. Huang, Q. Zhou, and B. Liu, *et al.*, *Nat. Commun.* **10**, 3461 (2019).
- [30] D. Zhou, D. V. Semenok, D. Duan, H. Xie, W. Chen, X. Huang, X. Li, B. Liu, A. R. Oganov, and T. Cui, *et al.*, *Sci. Adv.* **6**, eaax6849 (2020).
- [31] M. Peña-Alvarez, J. Binns, A. Hermann, L. C. Kelsall, P. Dalladay-Simpson, E. Gregoryanz, and R. T. Howie, *Phys. Rev. B* **100**, 184109 (2019).
- [32] D. Zhou, D. V. Semenok, H. Xie, X. Huang, D. Duan, A. Aperis, P. M. Oppeneer, M. Galasso, A. I. Kartsev, and A. G. Kvashnin *et al.*, *J. Am. Chem. Soc.* **142**, 2803 (2020).
- [33] L. Ma, G. Liu, Y. Wang, M. Zhou, H. Liu, F. Peng, H. Wang, and Y. Ma, arXiv:2002.09900.

- [34] D. V. Semenov, I. A. Kruglov, I. A. Savkin, A. G. Kvashnin, and A. R. Oganov, *Curr. Opin. Solid State Mater. Sci.*, **24**, 100808, (2020).
- [35] Y. Wang, J. Lv, L. Zhu, and Y. Ma, *Comput. Phys. Commun.* **183**, 2063 (2012).
- [36] Y. Wang, J. Lv, L. Zhu, and Y. Ma, *Phys. Rev. B* **82**, 094116 (2010).
- [37] B. Gao, P. Gao, S. Lu, J. Lv, Y. Wang and Y. Ma, *Sci. Bull.* **64**, 301 (2019).
- [38] L. Zhu, H. Liu, C. J. Pickard, G. Zou, and Y. Ma, *Nat. Chem.* **6**, 644 (2014).
- [39] G. Kresse and D. Joubert, *Phys. Rev. B* **59**, 1758 (1999).
- [40] G. Kresse and J. Furthmüller, *Phys. Rev. B* **54**, 11169 (1996).
- [41] J. P. Perdew, K. Burke, and M. Ernzerhof, *Phys. Rev. Lett.* **77**, 3865 (1996).
- [42] P. Giannozzi, S. Baroni, N. Bonini, M. Calandra, R. Car, C. Cavazzoni, D. Ceresoli, G. L. Chiarotti, M. Cococcioni, and I. Dabo *et al.*, *J. Condens. Matter Phys.* **21**, 395502 (2009).
- [43] P. B. Allen and R. C. Dynes, *Phys. Rev. B* **12**, 905 (1975).
- [44] P. Strange, A. Svane, W. M. Temmerman, Z. Szotek, and H. Winter, *Nature* **399**, 756 (1999).
- [45] J. Jensen and A. R. Mackintosh, *Rare earth magnetism* (Clarendon Press Oxford, (1991).
- [46] A. Simon, *Angew. Chem. Int. Ed.* **36**, 1788 (1997).
- [47] E. R. Ylvisaker, J. Kuneš, A. K. McMahan, and W. E. Pickett, *Phys. Rev. Lett.* **102**, 246401 (2009).
- [48] S. Klotz, M. Casula, K. Komatsu, S. Machida, and T. Hattori, *Phys. Rev. B* **100**, 020101 (2019).
- [49] W. M. Temmerman, Z. Szotek, A. Svane, P. Strange, H. Winter, A. Delin, B. Johansson, O. Eriksson, L. Fast, and J. M. Wills *et al.*, *Phys. Rev. Lett.* **83**, 3900 (1999).
- [50] C. Wang, S. Yi, and J. H. Cho, *Phys. Rev. B* **100**, 060502 (2019).
- [51] N. P. Salke, M. M. Davari Esfahani, N. Yedukondalu, Y. Zhang, I. A. Kruglov, J. Zhou, E. Greenberg, V. B. Prakapenka, J. Liu, and A. R. Oganov *et al.*, *Inorg. Chem.* **59**, 5303 (2020).